Low-Frequency processes and turbulence structure in a perturbed boundary layer

L. Mortarini, E. Ferrero, S. Falabino, S. Trini Castelli,
R. Richiardone and D. Anfossi
Study of the turbulence structure in the boundary layer over an urban area.

Quarterly Journal of the Royal Meteorological Society
Volume 139, Issue 673, Year 2013, pp. 1059–1072, DOI: 10.1002/qj.2015.

Study of the turbulence structure in the boundary layer over an urban area

L. Mortarini,[a] *E. Ferrero [b] S. Falabino [c] S. Trini Castelli [c] R. Richiardone [c] D. Anfossi[a]

[a] *Institute of Atmospheric Sciences and Climate, CNR, Torino, Italy* [b] *Department of Science and Advanced Technologies, University of Piemonte Orientale, Alessandria, Italy* [c] *Department of General Physics, University of Torino, Torino, Italy*

*Correspondence to: Institute of Atmospheric Sciences and Climate, National Research Council, Torino, Italy.Tel.: +39-3839835, Fax: +39-011-6600364 E-mail: l.mortarini@isac.cnr.it

An analysis of the turbulence structure in the urban boundary layer layer and in low-wind regime is presented. The study is based on 15-months of continuous wind and turbulence measurements gathered, in the frame of the Urban Turbulence Project, at three levels (5, 9 and 25 m) on a mast located in the city of Turin (Italy). The aim of the work is to investigate the influence of the urban environment on the turbulence structure, in the peculiar conditions of calm regime. In fact, the urban canopy and the heat island, together with frequent low-wind conditions, interact with and modify the turbulence structure. In order to investigate this modification, the velocity Eulerian auto-correlation functions, the Eulerian and Lagrangian time scales are shown and compared with the classical theory. The comparisons point out that in low-wind cases the velocity auto-correlation functions are not simply exponential but present an oscillating behavior. A new method of normalization is proposed together with an analysis on the applicability of this function. The estimated Lagrangian time scales are compared with two widely used parametrizations. It is found that the presence of the urban fabric influences the turbulence time scales and suggests the development of new parametrizations. Finally, higher-order statistics are evaluated and the relationship between higher and lower order moments are analysed pointing out the effects due to the urban environment.

Key Words: Urban boundary-layer; Turbulence structure; Data analysis; Low-wind

Received . . .

Citation: . . .

1. Introduction

As it is well known, the flow and turbulence structure of the atmospheric Boundary Layer (BL) above urban areas is significantly perturbed by the presence of the canopy and of the heat island (see: Kastner-Klein and Rotach 2004; Rotach 1999; Roth 2000, for a review). Thus it has to be expected that the classical theories of the BL turbulence, which generally refer to horizontally homogeneous conditions over flat terrain, cannot properly fit observations carried out in an urban environment.

A picture of the differences between BL developing over a smooth surface and over a rough surface was given in laboratory experiments by Ferrero *et al.* (2009c); Raupach *et al.* (1986). However, detailed turbulence measurements in real atmosphere are hardly available. To investigate these peculiar conditions a 15-months field campaign was conducted in the city of Turin (Italy), in the frame of the Urban Turbulence Project (UTP, Ferrero *et al.* 2009a; Mortarini *et al.* 2009). Three sonic anemometers were placed on a mast and the wind velocity components at different levels (5 m, 9 m and 25 m) were recorded and processed. It was found that the measurement site is characterized by very frequent low-wind speed conditions (more than 80% data with $\overline{u} < 1.5$ m s^{-1} at 5 m). When these conditions occur low frequency (typically 30 - 60 minutes) horizontal wind oscillations cause the

meandering of the mean wind direction. Furthermore, in this case, the wind velocity autocorrelation functions do not fit an exponential decay but show an oscillating behavior (Anfossi *et al.* 2005) probably determined by horizontal coherent structures (Veneziani *et al.* 2004). The presence of organised turbulence structures in the BL can also be related to the non-locality of the turbulence dynamics. As a matter of fact, in previous works, it was found through higher order moments analysis, that the turbulence transport is a non-local phenomena, not only in the convective BL (Canuto *et al.* 1994; Cheng *et al.* 2005; Colonna *et al.* 2009; Ferrero and Colonna 2006; Gryanik and Hartmann 2002) but also in the neutral (Ferrero 2005; Ferrero and Racca 2004) and in the stable (Ferrero *et al.* 2009b) ones. However, the urban BL has not been satisfactorily investigated from this point of view, as well as the low-wind conditions, which can also occur in the urban environment. Furthermore, fourth order moments (FOMs) have rarely been evaluated in open field (Gryanik and Hartmann 2002) and their Gaussianity still remains matter of discussion. In the present paper, an investigation of the turbulence structure in an urban BL is proposed and the differences with the usual formulations used for describing the turbulence in a BL over flat terrain and windy condition are highlighted. Flat terrain and windy condition are the common ground of classical (theories as the Monin-Obukhov Similarity Theory). The feasibility of these theories and of the turbulent parametrizations derived from them in low-wind conditions and in the urban fabric may then be questionable, as suggested by Roth (2000).
The turbulence structure in the urban BL is analysed starting from the wind velocity components measurements at three different levels, carried out in the frame of the Urban Turbulence Project (UTP). The length of the dataset allows us to consider the turbulence characteristics in different stability and wind conditions. The aspects we are dealing with are the correlation functions, the Lagrangian time scales and the higher order moments of the velocity probability density function (PDF). All these quantities show different behavior with respect to the open space case. Analysing the horizontal time-correlation functions we found that they show a peculiar oscillating trend with a significant negative lobe due to the low-wind regime, confirming the results of Anfossi *et al.* (2005). The presence of obstacles seems not to interfere with the correlation function behavior, but plays an important role in reducing the meandering time scale. With respect to the rural situations, the Lagrangian time scale analysis indicates that in the examined urban environment, in stable and unstable conditions, the size of the eddies is modified. The presence of turbulent structures in the BL is also studied through the Quasi-Normal (QN) approximation (Hanjalic and Launder 1972, 1976; Zeman 1981) or Eddy Damped Quasi Normal Markovian approximation (Lesieur 2007), or Millionshchikov Hypothesis (Monin and Yaglom 1971). As pointed out by Gryanik and Hartmann (2002), the non-Gaussianity of FOMs derives from the contribution of semi-organized structures responsible for the non-local transport. The higher order moments of turbulence evaluated from the UTP data fail to verify this approximation, especially at the lower levels, implying that the closest buildings of the urban fabric generate turbulence structures and enhance the non-locality of the flow in the BL. Section 2 is devoted to the field campaign and collected data-set presentation. In Sections 3, 4, 5 and 6 the data analysis and the results are described. Finally in Section 7 the main conclusions are summarised.

2. The UTP field campaign and estimated parameters

The UTP experiment was held in the city of Turin located at the western edge of the Po Valley at about 220 m a.m.s.l. A hill chain (maximum altitude of about 700 m a.m.s.l.) surrounds Turin on the eastern sector while the Alps (whose crest line is about 100 km distant) encircles it in the other three sectors. The CNR station is a meteorological station held by the Physics Department of the University of Turin.

The area where the instruments are located is in the southern outskirts of the town on grassy, flat terrain surrounded by buildings (Figure 1). It is characterized by about 30-m-tall buildings 150 m in the north-northeast direction and by sparse low buildings (from 4 m to 18 m) at a distance between 70 m to 90 m in the other sectors. Turin, which is in the western part of the Po Valley, is characterized by frequent occurrences of low-wind speed conditions (about 90% of the time).

A 25 m mast, equipped with horizontal booms pointing West and East at 5 m, 9 m, 25 m height, is located at the centre of the station. Two booms pointing North and South are installed at 25 m height, too. The three anemometers were respectively two Solent 1012R2, placed at 5 m and 9 m, and a Solent 1012R2A at 25 m (for a more detailed description of the equipment see Ferrero *et al.* 2009a). The UTP measurement campaign commenced on 18 January 2007 and besides some interruptions for maintenance, the three anemometers worked continuously for 15 months. The data considered in this work were stored with a frequency of 20 Hz. More details about the measurements are given in Mortarini *et al.* (2009); Trini Castelli *et al.* (2011).

3. Eulerian auto-correlation functions

The Eulerian time auto-correlation functions (EAFs), $R_i(\tau)$, are evaluated from 1-hour datasets. To avoid statistical noise, a decimation of raw data was carried out by computing the mean of each subset of 10 data, thus obtaining a final series of 7200 data sampled at 0.5 s intervals. $R_i(\tau)$ $(i = u, v, w)$ was computed from:

$$R_i(\tau) = \frac{\overline{u_i(t)u_i(t+\tau)}}{\sigma_i(t)} \tag{1}$$

In literature it is common to consider an EAF of the form:

$$R_i(\tau) = e^{-\frac{\tau}{T}} \tag{2}$$

where T is the characteristic time scale, which is often estimated considering the value for which $R_i(\tau)$ is equal to $1/e$ (Anfossi *et al.* 2000; Hanna 1981; Kaimal and Finnigan 1994). Eq. 2 can be proved true for the vertical component but it is a less general result for the two horizontal components.
In previous studies (Anfossi *et al.* 2005; Oettl *et al.* 2005), low-wind sonic anemometer data collected in flat terrain (Tisby, Sweden) and in complex terrain (Graz, Austria) were analysed. The main results were:

- The Eulerian autocorrelation functions (EAFs) of horizontal wind components show an oscillating behavior with the presence of large negative lobes due

to the meandering. The observed EAFs, $R(\tau)$, were correctly fitted by the following relationship:

$$R(\tau) = e^{\frac{-\tau}{(m^2+1)T}} cos\left[\frac{m\tau}{(m^2+1)T}\right] \quad (3)$$

proposed by Frenkiel (1953). This may also be written (Murgatroyd 1969) as:

$$R(\tau) = e^{-p\tau} cos(q\tau) \quad (4)$$

by setting

$$\begin{cases} p = \dfrac{1}{(m^2+1)T} \\ q = \dfrac{m}{(m^2+1)T} \end{cases} \quad (5)$$

- Both Eqs. 3 and 4 contain two parameters: T (or p) associated to the classical Eulerian integral turbulence time scale, m (or q) associated to the meandering characteristics.
- The meandering period was defined as:

$$T_* = \frac{2\pi T(m^2+1)}{m} = \frac{2\pi}{q} \quad (6)$$

- It was also found that the minimum value (R_{min}) of Eqs. 3 and 4 has the following expression

$$R_{min} = -\frac{exp\left\{-\left[-arctan(\frac{1}{m}) + \pi\right]\frac{1}{m}\right\}}{\sqrt{1+m^2}} m \quad (7)$$

from which it appears that R_{min} depends upon $m = q/p$ only. It was found that the observed R_{min} increases as the average wind speed approaches zero.
- Oettl *et al.* (2005) and Goulart. *et al.* (2007) also provided a new physical explanation of the meandering occurrence. Meandering is explained as an inherent property of atmospheric flows in low-wind speed conditions that, generally, does not need any particular trigger mechanism to be initiated. Meandering is shown to arise when the 2-D flow approaches or nearly approximate geostrophic balance, and it is damped out and vanishes when the Reynolds stresses are larger.
- According to those works, meandering seems to exist under all meteorological conditions regardless the atmospheric stability, specific topographical features, or season.

With reference, in particular, to the latter point, in the present paper we wanted to verify if the same results could be also found in an urban site. Therefore, EAFs were calculated at the three mast levels, by way of direct computation (Eq. 1) on the hourly horizontal wind series. Then, for each horizontal EAF (u and v), a non-linear best fit to Eqs. 3 and 4 provided the m, T or p, q values.

Figure 2 shows the R_{min} values estimated from the computed EAFs at 5 m as a function of m for the two horizontal EAF components. Theoretical eq. 7 is plotted as a continuous line. To plot Figure 2 only stationary data were used. The stationarity was tested applying the reverse-arrangement stationarity test suggested in Bendat and Piersol (2000). It can be observed that eq. 7 fairly well fits the calculated R_{min} values, even if with a large spread. We also notice that for $m \sim 1$ the R_{min} value attains values $\sim -0.1/-0.2$, i.e. significantly negative. This suggests to choose $m = 1$ as the limiting value to define the low-wind regime. It is worthwhile to observe that this definition is valid in general, i.e not only in urban conditions. We recall that Anfossi *et al.* (2005) observed that there is not a general consensus in the literature on how to define low-wind speeds. This definition is based on a limiting wind speed that ranges from 0.5 m s^{-1} to 2.0 m s^{-1} and they suggested 1.5 m s^{-1} as a tentative value on the basis of subjective examination of many EAFs. Thus, as an alternative or complementary option, we propose to operatively consider as low-wind regime those cases in which $m \geq 1$.

Then, the average EAFs were computed at the three levels. Only the cases in which $\overline{u} < 1.5$ m s^{-1} and $m \geq 1$ were included. The average EAFs for the u and v components for the 5 m height are shown in Figure 3. The left panel plots the average $R(\tau)$ vs τ, whereas in the right panel each EAF was scaled by its meandering period T_* (i.e. τ/T_*) before averaging. Solid lines refer to the average u and v components EAFs and dashed lines indicate $\pm$ a standard deviation (sd). Similar results were obtained for 9 m and 25 m.

We observe that the three curves, average u-EAF, u-EAF+sd, u-EAF-sd, and the three corresponding v-EAFs are almost coincident. This underlines the fact that, since in low-wind conditions there is not a well definable mean wind direction, the distinction between along-wind and cross-wind components in the averaged EAFs disappears. We also notice that when the x-axis is not scaled for the single EAFs, left panel, the average EAF has a small negative lobe and the different oscillation frequency of each EAF mixes in the average one. On the contrary, when the x-axis is scaled for the single EAFs, right panel, all EAFs and, consequently, their average EAF collapse on the same oscillating period and shows the typical low-wind oscillating behavior of the single EAFs. In particular, R_{min} of the averaged EAF is about -0.4 and it fluctuates from -0.6 to -0.2. Zeroes of the non-dimensional time τ/T_* occur at $\tau/T_* = 0.25 + 0.5k$ (k any integer) for which $cos\left[q\left(\frac{\pi}{2} + k\pi\right)\frac{1}{q}\right] = cos(\frac{\pi}{2} + k\pi)$=0.

Table I shows the average p and q values, the meandering periods and the standard deviations obtained by fitting the two wind components u and v for the stable, unstable and all cases. Columns 2, 4 and 6 indicate the number of EAFs considered, respectively. The fact that the number of cases, for the same stability, is different for the two components is due to the imposed condition: $m \geq 1$. We observe that the average p, q and T^* values are almost the same for both wind components and that their standard deviations are large. The p and q values are larger in unstable conditions than in stable ones, while the opposite occurs for the meandering period. T^* is of the order of 1500 - 1600 s, not so different from what found by Anfossi *et al.* (2005), $T^* \sim 2000$ s for the v-component in a rather flat terrain. This reduction in the meandering time scale may be related to the effect of the urban canopy. This can be interpreted according to Goulart. *et al.* (2007). They showed that assuming low-wind speed and negligible turbulent forcing, the Navier-Stokes equations provide an asymptotic meandering solution. Instead, if the turbulent forcing increases, the horizontal Reynolds-stress terms cause the horizontal wind components disconnecting

Table I. p and q average values at 5 m values for the two wind components and their standard deviations computed at 5 m. N indicates how many data have been used to evaluate the parameters.

	stable		**unstable**		**all**	
parameter	N	value	N	value	N	value
p_u [s^{-1}]	1636	0.00195	1609	0.00326	3613	0.00257
q_u [s^{-1}]		0.00491		0.00632		0.00557
σ_{pu} [s^{-1}]		0.00303		0.00451		0.00390
σ_{qu} [s^{-1}]		0.00220		0.00380		0.00310
T_u^* [s]		1641.9		1432.9		1547.5
$\sigma_{T_u^*}$ [s]		727.6		764.0		751.6
p_v [s^{-1}]	1686	0.00209	1765	0.00284	3482	0.00246
q_v [s^{-1}]		0.00515		0.00582		0.00546
σ_{pv} [s^{-1}]		0.00415		0.00472		0.00441
σ_{qv} [s^{-1}]		0.00325		0.00978		0.00362
T_v^* [s]		1634.6		1494.4		1570.2
$\sigma_{T_v^*}$ [s]		727.4		734.8		734.4

from each other, which breaks the undulating behavior associated with the meandering phenomenon. Thus we can infer that the urban canopy slightly increases the turbulent forcing of an amount such that the low-wind speeds are not enough to destroy the meandering but act in reducing the meandering time.

Besides the meandering time scale, also the Eulerian integral time scale can be obtained from Eqs. 3 or 4 (Anfossi *et al.* 2005):

$$T_E = \int_0^\infty R(\tau)d\tau = \frac{p}{p^2+q^2} = T \tag{8}$$

Substituting the first of Eqs. 5 inside Eq. 8 a relationship between the Eulerian time scale and the meandering parameter m is easily found:

$$T_E = \frac{m}{q(1+m^2)} \tag{9}$$

Figure 4 shows the dependence of T_E on m for the three levels together with the theoretical behavior of Eq. 9. q and m are not independent, therefore several parabolas should be plotted. The one showed has $q = q_{min}$, where $q_{min} = \frac{2\pi}{3600}$ is the minimum meandering frequency achievable considering one hour subset. As expected, the values are concentrated on the right hand side of the plot where $m \geq 1$, i.e. where the meandering parameter m is larger. This gives some further evidence that a condition on the wind speed, for example $\overline{u} < 1.5$ m s^{-1}, is not enough to justify an oscillating behaviour for the horizontal EAFs. An additional condition of m should be given and, accounting also for the results in Figure 2, we definitely propose to use $m \geq 1$. A convincing argument for $m \geq 1$ comes from Eq. (7). The value of the first negative lobe can be used as a discriminant between the oscillating behavior and the exponential decay. It can be easily verified that significant values of R_{min} ($R_{min} < -0.1$) occur for $m > 1$.

4. Eulerian and Lagrangian times scale.

In order to compare the estimated time scales with the parametrizations it is necessary to move from Eulerian to Lagrangian time scales, since the literature presents parametrizations for the latter in the surface layer or in the atmospheric BL. It is to remember that the estimation of the ratio between the Lagrangian and the Eulerian time scales, $\beta = T_L/T_E$, is an open problem (e.g. Anfossi *et al.* 2006a,b). In windy conditions the generally accepted expression is (Hay and Pasquill 1959):

$$\beta = \gamma\overline{u}/\sigma = \gamma/i \tag{10}$$

where $i = \sigma/\overline{u}$ is the turbulence intensity and γ is a numerical coefficient. In this work we use $\gamma = 0.55$ as suggested by Degrazia and Anfossi (1998). However, in low-wind conditions Eq. 10 does not apply, as for $\overline{u} \to 0$ the ratio T_L/T_E tends to zero. Anfossi *et al.* (2006b), by using Large Eddy Simulations (LES), demonstrated that other expressions with a finite non-zero value for $\overline{u} = 0$ fit equally well their LES data. Anfossi *et al.* (2006a) examining low-wind data used the following β expression:

$$\beta = 0.25 + 0.39\overline{u}/\sigma = 0.25 + 0.39/i \tag{11}$$

and found $\beta = 1.00 \pm 0.35$. Therefore, accounting for these considerations in the present analysis the two β expressions (Eqs. 10, 11) were utilized for transforming time scales from Eulerian to Lagrangian frames. Equation 11 was used for data with $\overline{u} < 1.5$ m s^{-1} and meandering coefficient $m \geq 1$, whereas Eq. 10 was used for the other cases.

As an example, in Figures 5 and 6 the Lagrangian time scales estimated at 25 m are compared with two turbulence parametrizations widely used in dispersion models: Hanna (1982) and Degrazia *et al.* (2000). The Hanna (1982) parametrization provides the time scales as a function of the boundary-layer and surface-layer parameters, while Degrazia *et al.* (2000) derive their expressions on the basis of observed turbulence spectra and on Taylor's statistical diffusion theory. The Lagrangian time scales evaluated at the other two levels show a similar behaviour. Both Figures 5(a) and 5(b) show, as a function of stability, the ratios ρ_{T_L} between the Lagrangian time scales evaluated by the two parametrizations and the the time scale (T_{LData}) evaluated from the auto-correlation function. In order to show the variability of the time scale inside each stability class we preferred to plot the boxplots instead of single points. The whiskers extend from the lowest datum still within 1.5 times the interquartile range of the lower quartile, to the highest datum still within 1.5 times the interquartile range of the

upper quartile. The comparison with T_L estimated from data shows that the Degrazia *et al.* (2000) parametrization over-estimates in unstable conditions and under-estimates in stable conditions. For the u-component (Figures 5(a)) Hanna (1982) parametrization has a good agreement for very stable data but it over-estimates in unstable conditions. For the w-component (Figures 5(b)) the agreement is good for neutral cases and worsens with increasing stability, whereas in unstable cases the parameterized time scales are slightly less than twice the ones evaluated from the auto-correlation functions.

To better compare these data and to take into account the high variability shown by the boxplots, the probability distributions can be compared with quantile-quantile (q-q) plots. Figure 6 show the q-q relationships between the T_L (u component) parameterized and the one evaluated with the auto-correlation functions at 25 m (along each axis the respective boxplot is shown to provide insight of the cumulative density function and the data distribution around the median value). Figure 6 shows that the two parametrizations have different probability density functions, especially for large values of T_L. Hanna (1982) parametrization fits the data quite well in the interquartile range, but it over-estimates the data for large values, while the Degrazia *et al.* (2000) T_L and the ones obtained from the autocorrelation function are in good agreement only in the lower percentiles, for small T_L values. Looking at these results, one may wonder if the differences between the two T_L parametrizations and the present results might be influenced by our choice of β (Eq. 11 instead of Eq. 10) for the low-wind cases. In fact, both parametrizations make use of eq. 10 to transform the Eulerian time scales, more easily computable from measurements, into the Lagrangian ones; however, Hanna (1982) parametrization used a slightly different numerical coefficient, 0.6. Examining in detail this possibility we found the following ranges of values for the mean ratio (Eq. 11 over Eq. 10) between the two estimates β_{LW} (for low-wind cases) and β_W (for windy cases): $1.04 < \beta_{LW}/\beta_W < 1.06$ at 5 m, $0.95 < \beta_{LW}/\beta_W < 1.00$ at 9 m and $0.86 < \beta_{LW}/\beta_W < 0.94$ at 25 m. These ratios are not significantly different from 1 and, in any case, not sufficient to justify the differences shown in Figure 5. β_{LW} and β_W values, were found to be ~ 0.75 at 5 m (for both u and v component and stable and unstable cases), included between 0.80 and 1.00 at 9 m and included between 1.00 and 1.60 at 25 m (the highest in the stable case and for the v component). We also observe that β values greater than 1 were only found at 25 m. This is not surprising because at 25 m a larger number of windy cases was detected: 40%, whereas the corresponding numbers for 9 and 5 m are 14% and 8%, respectively. In fact, in general, $\beta > 1$ is "intuitively reasonable since the time required by a balloon to completely pass around an eddy would be longer than the time required by the same eddy to be transported past a fixed anemometer by the mean wind " (Hanna 1981). On the contrary, in simulations without a mean flow, values less than 1 were found (Anfossi *et al.* 2006b). The occurrence of $\beta < 1$ can be easily explained considering that, in cases with no mean flow, the horizontal wind fluctuation standard deviation is greater than about twice the mean horizontal wind speed.

It is also worthwhile to underline that both Hanna (1982) and Degrazia *et al.* (2000) parametrizations were not derived for low-wind speed and urban conditions. Thus, significant differences could have been expected. The present comparison shows that, at least for the horizontal components, the Lagrangian time scales evaluated from the data are significantly different from the Hanna (1982) and Degrazia *et al.* (2000) parametrizations in unstable conditions. This suggests that even if the stability is one parameter to be considered, low-wind occurrences can be very important as well. A new T_L parametrization appropriate to these conditions is needed.

5. High-Order Statistics

In the statistical approach of the turbulence, higher order moments such as skewness and kurtosis should be considered. As a matter of fact, these quantities specify important characteristics of the velocity PDF as, for example, the turbulent transport and the intermittency. Furthermore turbulence models need closures which are generally prescribed as relationships between higher and lower order moments (Ferrero *et al.* 2008; Gryanik and Hartmann 2002; Lesieur 2007). Despite their importance it is difficult to find turbulence higher order moments data in the literature. Therefore in this Section we present and discuss the relationship between higher and lower order moments and the relationship between skewness and kurtosis. The QN approximation is the most used among these relationships. It postulates that the FOMs can be expressed as a combination of the second order moments assuming a Gaussian distribution:

$$\overline{a'b'c'd'} = \overline{a'b'}\ \overline{c'd'} + \overline{a'c'}\ \overline{b'd'} + \overline{a'd'}\ \overline{b'c'}, \qquad (12)$$

where the letters a, b, c, d represent turbulent variables (in our case the velocity components) and the prime indicates their fluctuations. Since turbulence distributions are usually non-Gaussian, one cannot expect a simple Gaussian-like relationship between 2^{nd} and higher moments. The validity of the QN approximation is not yet proved in real flows characterised by different stability conditions. An analysis of the QN approximation was carried out by Ferrero *et al.* (2008), who performed a series of experiments in a turnable water tank with different roughnesses and different rotation speeds. Moreover, QN approximation is widely adopted in turbulence models with the purpose to close the fourth order moments (Canuto 1992; Ferrero 2005). The relationship expressed in Eq. 12 can be verified using second order moments (SOMs) and FOMs obtained from the sonic anemometer measurements. For this purpose we considered some FOMs compared with the expression obtained from the QN approximation as a function of the measured SOMs in different stability and wind speed conditions.

The observations of high order moments are often scattered and their evaluation is difficult (Lenschow *et al.* 1994). In order to reduce the statistical noise in this section only stationary data (i.e. the 25% of the data for the 5 m measurement, the 30% and 31% for the 9 m and 25 m levels) were considered.

In Figures 7 the q-q plots of the velocity fluctuations FOMs ($\overline{u'^4}$, $\overline{v'^4}$, $\overline{u'^3w'}$ and $\overline{w'^4}$), with the corresponding QN approximations, are shown for the three levels. On the top and the side of each figure the boxplot of the data gives an insight of the distribution of the data around their median value. All the wind and stability conditions are accounted for in these plots. As far as the 25 m measurement is concerned, the QN approximation for the two horizontal components agrees with the FOMs, except for a slight

underestimation at the higher values for the u-component. On the contrary, the QN approximation underestimates the measured $\overline{u'^4}$ and $\overline{v'^4}$ for values of these quantities greater than 2.5 m^4 s^{-4}. Being outside the domain contained by the boxplots these values represent a small number of cases and may not be representative. Looking at the FOM of the vertical component, it can be observed that the QN approximation underestimates the FOM even inside the boxplots domain and the worse agreement is found at the lower levels. Generally speaking, we can say that $\overline{w'^4}$ does not present Gaussian values but it attains larger ones. This may imply that the turbulent velocity fluctuations are larger than in Gaussian turbulence. This fact can be related to the particular conditions of the experiments (urban environment, frequent low-wind and stable stratification, which cause turbulence intermittency). In the horizontal directions the QN approximation seems to be a correct model for the FOM at lower values, when turbulence intensity is reduced and the Gaussian PDF is more likely to correspond to the real one. Among the other FOMs, Figure 7 shows also the moement $\overline{u'^3w'}$, which represents the vertical flux of the horizontal skewness and could be an important parameter in describing the non-locality of the flow. Also in this case the agreement between the QN approximation and the calculated FOMs is rather good inside the boxplots intervals, with a small underestimation for the 25 m measurement and a small overestimation for the 5 m and 9 m measurements.

In the next Figure (8) a deeper investigation is presented in term of boxplots of the ratio between FOMs and QN approximation, as a function of the stability and for the three levels. The FOMs exibits a larger spread around the median in stable conditions. Concerning the two FOMs $\overline{u'^4}$ and $\overline{w'^4}$ (Figures 8(a) and 8(b)) the agreement between FOMs and QN approximation is better for the u-component. As regards the w-component, measurements overestimate the QN approximation in the whole stability range, but in the stable conditions the departure from the Gaussian behavior is particularly evident. The agreement is better at 25 m while at the lower levels it gets worse, suggesting the influence of the ground proximity on the departure from the Gaussian values. The moment $\overline{u'^3w'}$ (Figure 8(c)) agrees with the QN approximation in unstable conditions, while it shows some discrepancies in stable conditions. In conclusion, it results that the larger departures from the Gaussian distribution appear in stable conditions and close to the ground. This is a remarkable fact, since in this conditions Gaussian distribution is generally assumed as a good model for the velocity components PDF. On the contrary, unstable conditions are generally considered to be far from this model due to the presence of the downdrafts and updrafts that gives a non zero skewness. Also, it can be noted that, since the stable conditions are often related to low-wind conditions, these could be the cause of QN approximation failure.

The same analysis but as a function of the wind intensity is presented in Figure 9. It can be observed that at all the levels $\overline{w'^4}$ (Figure 9(b)) QN approximation underestimates the corresponding FOM, especially for low-wind conditions, and that $\overline{u'^4}$ and $\overline{u'^3w'}$ (Figures 9(a) and 9(c)) generally agree, except for the 5 m measurements, in the range between 2 and 4 m s^{-1}.

6. Skewness-Kurtosis relationship

Looking for an expression of FOMs as a function of lower order moments, a different choice with respect to the QN approximation can be made by resorting to a relationship between kurtosis (K) and skewness (S). On this subject the relevance of high-order statistics for the turbulent dispersion was discussed in Wyngaard and Weil (1991), Maurizi (2006) and Quan *et al.* (2012). It is well known that an inferior statistical limit for K, in the (S, K) space, exists: $K = (S^2 + 1)$ (Kendall and Stuart 1979), which bounds the Quasi-Normal Approximation in the range of S values. Tampieri *et al.* (2000) proposed the relationship:

$$K = \alpha(S^2 + 1) \tag{13}$$

with $\alpha = 3.3$ for a sheared flow. Maurizi (2006) demonstrated that K-values above this curve correspond to damping terms for the turbulent kinetic energy budget (dynamic stability) and related these values to stable conditions, suggesting a dependence of α on the stability, i.e. $\alpha(\frac{z}{L})$. Ferrero *et al.* (2008), in their experiments showed that an analogous effect is found when high rotation speed or low surface roughness are accounted for. Here we want to verify the effects of low-speed conditions and stability condition on the relationship between skewness and kurtosis.

In Figures 10(a) and 10(b) the vertical velocity kurtosis as a function of the skewness is depicted for low ($\overline{u} <$ 1.5 m s^{-1}) and strong ($\overline{u} >$ 1.5 m s^{-1}) wind conditions respectively. In Table II the values of the coefficient α, obtained by a best fit of Eq. 13, are shown. The data refer to the whole data set. The most part of them exhibits a consistent departure from the Gaussian value, nevertheless all the data are above the statistical limit. As far as the low-wind condition is concerned (Figure 10(a)), data of the lower layers have kurtosis values larger than those computed by Eq. 13 with $\alpha = 3.3$, while data of the 25 m measurement show smaller values of kurtosis. According to Ferrero *et al.* (2008) this can be due to the effect of the local surface characteristics at the mast which more largely affects the levels closest to the ground. In the case of higher wind (Figure 10(b)), kurtosis at all the levels decreases, giving values very close to the Gaussian one, confirming the increase of stability with lower winds. However the values of the coefficient α in Eq. 13 (Table II) do not exhibit remarkable differences among the different levels. About the skewness, we can observe that at the lower levels there is a larger number of negative cases, while at 25 m it is almost symmetrically distributed around zero. This result is found for both low and high wind conditions.

Figures 11(a) and 11(b) show the same plots but for different stability conditions. The results for the unstable case, $(-2 < z/L < -0.01)$ demonstrate that only some of the points corresponding to the lower level are well above the dashed line indicating Eq. 13 ($\alpha = 3.3$), while in the other cases distribute in a symmetrical way around it and the points are close to the Gaussian value. Looking at the stable cases $(0.01 < z/L < 2)$, it is found that, as expected, on average the measured data are displaced above the curve given by Eq. 13 much more than in the unstable case and their spread is larger. As a matter of fact, values of kurtosis above this curve indicate stability as suggested by Maurizi (2006). The values of the coefficient α in Eq. 13 obtained from best fits of the anemometer's data are summarised in Table II. It can be observed that the values of coefficient α

is larger in the stable cases.
The analysis of the higher order statistics points out that the relationships between fourth and second order moments and between skewness and kurtosis depend not only on the stability conditions, as generally could be expected, but also on the wind intensity. Furthermore different results are found at the different heights, although they are all in the surface layer. These findings suggest that higher order statistics is sensibly influenced by the presence of the urban fabric and by the peculiarities of the wind regime. In the analysed conditions, the QN approximation is hardly verified and both skewness and kurtosis show non-Gaussian values. This suggests that the turbulent flow is non-local, implying the presence of semi-organised structures.

7. Conclusions

In this work, data collected by three sonic anemometers installed at 5 m, 9 m ad 25 m along a meteorological mast 25 m high, in the Turin outskirt (Italy), during a 15-months experimental campaign, were analysed in order to study the turbulence structure in an urban environment characterized by frequent low-wind conditions. The present analysis was focused on studying some aspects of the atmospheric turbulence in urban areas and highlights the difference with the usual considered BL over flat terrain and windy condition. As it was found in previous analysis of low-wind data sets (Anfossi *et al.* 2005), also for the present data set the complexity of the urban structure has lower influence on the shape of the Eulerian Autocorrelation Functions and on the time scales than the frequent occurrence of low-wind speed conditions, while the presence of the urban fabric seems to influence the higher order statistics. The average meandering time was here found of the order of 1500 - 1600 s, whereas in the Tisby data set, collected in a rather flat terrain, the v-component value was of the order of 2000 s. This reduction in the meandering time scale may be related to the effect of the urban fabric, which, without inhibiting the meandering, increases the turbulent forcing and reduces the meandering time. As in previous studies (Anfossi *et al.* 2005), it was also found that in low-wind conditions the distinction between along-wind and cross wind components in the averaged EAFs disappears. This can be related to the fact that in these conditions it is not easily definable a mean wind direction.
An interesting way to show the horizontal EAFs, averaged over all the data set, was presented. It is based on the scaling of the lag time by the meandering period. In this way the average EAF collapse on the same oscillating period. It can be observed that R_{min} of averaged EAFs ranges from -0.2 to -0.6. This confirms that the meandering time is the predominant scaling time in the low-wind meandering phenomenon, i.e. the more energetic horizontal atmospheric oscillation.
A remarkable result concerns the definition of the low-wind speed regime. In a previous analyses (Anfossi *et al.* 2005), it was assumed $\overline{u} < 1.5$ m s^{-1} as the threshold value for the mean wind speed. In this paper we found that the computation by means of Eq. 7 of the minimum values (R_{min}) of the two horizontal EAF components showed that Eq. 7 correctly fits the observed R_{min} and that R_{min} values of about -0.1 are found for $m \sim 1$. These results suggest to propose $m \geq 1$ as a second conditions for defining the low-wind regime. It is worth noticing, that being based on Eq. 7, the last two points can be considered not related to the urban conditions but general results, although they were never found before.
The analysis of the Lagrangian time scale, when compared to two parametrizations from literature, Hanna (1982) and Degrazia *et al.* (2000), leads to the following conclusions. As far as the horizontal components are concerned, during the night, or in general in stable conditions, when the turbulence is suppressed and small $T_L s$ values are expected, both parametrizations (developed for flat and open terrain) underestimate the $T_L s$ derived from measurements, while in unstable conditions they overestimate of about a factor of two. Regarding the vertical component, Degrazia *et al.* (2000) parametrization behaves like in the horizontal ones, whereas the Hanna (1982) parametrization overestimates (a factor of about 1.5) in unstable conditions and underestimates in stable conditions. Thus the effect of the urban environment seems to be the reduction of the buoyancy action with respect to same condition in rural environment, maintaining relatively large scale eddies in stable conditions and limiting their size in unstable conditions.
As far as the higher order moments analysis is concerned, generally speaking the QN approximation is not verified, especially at the lower levels, where the presence of the closest buildings may influence the flow possibly generating turbulence structures. While in convective conditions it is to be expected that turbulence would not be Gaussian, in neutrally and stably stratified flow the QN approximation reasonably reproduces the FOMs (Ferrero *et al.* 2008). From the present analysis of the stability effects we found that the QN approximation fails in stable conditions and not in the unstable conditions This result can be due to the fact that unstable conditions are mainly generated by the mechanical turbulence instead of buoyancy. Looking at the effect of the wind speed intensity, the study has revealed that QN approximation satisfactorily fits the FOMs only for intense wind while it fails in low- or moderate-wind conditions. Then we analysed the $K - S$ relationship. It was found that the low-wind conditions are favorable for a non-Gaussian relationship giving kurtosis larger that in the Gaussian case. Asymmetrical values of the skewness found at the lower layer may indicate the influence of the urban fabric on the flow. Also in this case unstable conditions seem to be more compatible with a Gaussian relationship between skewness and kurtosis, suggesting that mechanical turbulence prevails upon the buoyancy in these conditions. All the results presented demonstrate the presence of organized turbulent structures. The Lagrangian time scales analysis demonstrated that some of this structures are related to low-wind conditions, while the evidence of the enhancement of the non-local transport shows that these structures are also related to the particular urban environment. This may have non negligible consequences on the turbulence models and the dispersion parameters, which should account for the effects of both low-wind and the urban fabric.

References

Anfossi D, Alessandrini S, Trini Castelli S, Ferrero E, Oettlt D, Degrazia G. 2006a. Tracer dispersion simulation in low wind speed conditions with a new 2-D langevin equation system. *Atmospheric Environment* **40**: 7234–7245.
Anfossi D, Degrazia G, Ferrero E, Gryanik V, Morselli M, Trini-Castelli S. 2000. Estimation of the lagrangian structure function constant C_0 from surface layer wind data. *Bound.-Layer Meteor.* **95**: 249–270.

Table II. Coefficients α from the best fit of Eq. 13.

Height	$\overline{u} < 1.5$ m s^{-1}	$\overline{u} > 1.5$ m s^{-1}	$-2 < z/L < -1$	$1 < z/L < 2$
5 m	3.91 ± 0.02	3.67 ± 0.03	3.42 ± 0.07	5.09 ± 0.14
9 m	3.55 ± 0.02	3.23 ± 0.02	3.01 ± 0.03	4.38 ± 0.13
25 m	3.88 ± 0.02	3.20 ± 0.01	2.94 ± 0.04	4.15 ± 0.11

Anfossi D, Mangia C, Rizza U, Degrazia G, Pereira Marques Filho E. 2006b. Estimation of the ratio between the lagrangian and eulerian time scales in the atmospheric boundary layer by large eddy simulation. *Atmospheric Environment* **40**: 326–337.

Anfossi D, Oettl D, Degrazia G, Goulart A. 2005. An analysis of sonic anemometer observations in low-wind speed conditions. *Boundary-Layer Meteorology* **114**: 179–203.

Bendat J, Piersol A. 2000. *Random data: Analysis & measurement procedures*. Wiley-Interscience Publishers: 598 pp, 3rd edn.

Canuto V. 1992. Turbulent convection with overshootings: Reynolds stress approach. *J. Astrophys.* **392**: 218–232.

Canuto V, Minotti F, Ronchi C, Ypma R, Zeman O. 1994. Second-order closure pbl model with new third-order moments: Comparison with les data. *J. Atmos. Sci.* **51(12)**: 1605–1618.

Cheng Y, Canuto V, Howard A. 2005. Nonlocal convective pbl model based on new third- and fourth-order moments. *J. Atmos. Sci.* **62**: 2189–2204.

Colonna N, Ferrero E, Rizza U. 2009. Nonlocal boundary layer: The pure buoyancy-driven and the buoyancy-shear-driven cases. *J. Geophys. Res.* **114**: D05 102.

Degrazia G, Anfossi D. 1998. Estimation of the Kolmogorov constant C_0 from classical statistical diffusion theory. *Atmospheric Environment* **32**: 3611–3614.

Degrazia G, Anfossi D, Carvalho J, Mangia C, Tirabassi T, Velho HC. 2000. Turbulence parameterisation for pbl dispersion models in all stability conditions. *Atmospheric Environment* **34**: 3575–3583.

Ferrero E. 2005. Third-order moments for shear driven boundary layers. *Bound.-Layer Meteor.* **116**: 461–466.

Ferrero E, Anfossi D, Richiardone R, Trini Castelli S, Mortarini L, Carretto E, Muraro M, Bande S, Bertoni D. 2009a. Urban turbulence project. the field experiment campaign. *Internal Report ISAC-TO/02-2009* : pag. 37.

Ferrero E, Colonna N. 2006. Nonlocal treatment of the buoyancy-shear-driven boundary layer. *J. Atmos. Sci.* **63**: 2653–2662.

Ferrero E, Colonna N, Rizza U. 2009b. Non-local simulation of the stable boundary layer with a third order moments closure model. *J. Mar. Sys.* **77**: 495–501.

Ferrero E, Genovese R, Longhetto A, Manfrin M, Mortarini L. 2008. Experimental study of higher-order moments in shear-driven boundary layers with rotation. *J. Fluid Mech.* **598**: 121–139.

Ferrero E, Mortarini L, Manfrin M, Longhetto A, Genovese R, Forza R. 2009c. Boundary-layer stress instabilities in neutral, rotating turbulent flows. *Boundary-Layer Meteorology* **130**: 347–363.

Ferrero E, Racca M. 2004. The role of the nonlocal transport in modelling the shear-driven atmospheric boundary layer. *J. Atmos. Sci.* **61**: 1434–1445.

Frenkiel F. 1953. Turbulent diffusion: mean concentration distribution in a flow field of homogeneous turbulence. *Adv. Appl. Mech* **3**: 61–107.

Goulart A, Degrazia G, Acevedo O, Anfossi D. 2007. Theoretical considerations of meandering wind in simplified conditions. *Boundary-Layer Meteorology* **125**: 279–287.

Gryanik V, Hartmann J. 2002. A turbulence closure for the convective boundary layer based on a two-scale mass-flux approach. *J. Atmos. Sci.* **59**: 2729–2744.

Hanjalic K, Launder B. 1972. A reynolds stress model of turbulence and its application to thin shear flows. *J. Fluid Mech.* **52**: 609–638.

Hanjalic K, Launder B. 1976. Contribution towards a reynolds-stress closure for low-reynolds-number turbulence. *J. Fluid Mech.* **74**: 593–610.

Hanna S. 1981. Lagrangian and eulerian time-scale in the daytime boundary layer. *J. Appl. Meteor.* **20**: 242–249.

Hanna S. 1982. Applications in air pollution modelling. In: *Atmospheric Turbulence and Air Pollution Modelling*, F Nieuwstadt HD (ed), F. Nieuwstadt, H.Van Dop: Reidel, Dordrecht, pp. 275–310.

Hay J, Pasquill F. 1959. Diffusion from a continuous source in relation to the spectrum and scale of turbulence. *Advances in Geophysics* **5**: 345–365.

Kaimal J, Finnigan J. 1994. *Atmospheric boundary layer flows*. Press, Oxford University.

Kastner-Klein P, Rotach M. 2004. Mean flow and turbulence characteristics in an urban roughness sublayer. *Boundary-Layer Meteorology* **111**: 55–84.

Kendall M, Stuart A. 1979. *The advanced theory of statistics, volume 2*. Griffin, London, 4th edition.

Lenschow D, Mann J, Kristensen L. 1994. How long is long enough when measuring fluxes and other turbulence statistics? *Journal of Atmospheric and Oceanic Technology.* : 661–673.

Lesieur M. 2007. *Turbulence in fluids*. Springer.

Maurizi A. 2006. On the dependence of third- and fourth-order moments on stability in turbulent boundary layer. *Nonlinear Processes in Geophysics* **12**: 119–123.

Monin A, Yaglom A. 1971. *Statistical fluid mechanics*, vol. 1. MIT Press.

Mortarini L, Ferrero E, Richiardone R, Falabino S, Anfossi D, Trini Castelli S, Carretto E. 2009. Assessment of dispersion parameterizations through wind data measured by three sonic anemometers in a urban canopy. *Adv. Sci. Res.* **3**: 91–98.

Murgatroyd R. 1969. Estimations from geostrophic trajectories of horizontal diffusivity in the mid-latitude troposphere and lower stratosphere. *Q. J. R. Meteorol. Soc.* **95**: 40–62.

Oettl D, Goulart A, Degrazia G, Anfossi D. 2005. A new hypothesis on meandering atmospheric flows in low wind speed conditions. *Atmospheric Environment* **39**: 1739–1748.

Quan L, Ferrero E, Hu F. 2012. Relating statistical moments and entropy in the stable boundary layer. *Physica A* **391**: 231–247.

Raupach M, Coppin P, Legg B. 1986. Experiments on scalar dispersion within a plant canopy, part i: the turbulence structure. *Boundary-Layer Meteorology* **35**: 21–52.

Rotach M. 1999. On the influence of the urban roughness sublayer on turbulence and dispersion. *Atmospheric Environment* **33**: 4001–4008.

Roth M. 2000. Review of atmospheric turbulence over cities. *Q. J. R. Meteorol. Soc.* **126**: 941–990.

Tampieri F, Maurizi A, Alberghi S. 2000. Lagrangian models of turbulent dispersion in the atmospheric boundary layer. In: *Ingegneria del vento in Italia 2000*.

Trini Castelli S, Falabino S, Mortarini L, Ferrero E, Anfossi D, Richiardone R. 2011. Analysis of urban boundary-layer turbulence on the basis of an experimental campaign in turin city utp project. *Proceedings of the 14th International Conference on Harmonisation within Atmospheric Dispersion Modelling for Regulatory Purposes, Kos, Greece, 2 6 October 2011* **391**: 414–417.

Veneziani M, Griffa A, Reynolds A, Mariano A. 2004. Oceanic turbulence and stochastic models from subsurface lagrangian data for the northwest atlantic ocean. *Journal of Physical Oceanography* **34**: 1884 – 1906.

Wyngaard J, Weil J. 1991. Transport asymmetry in skewed turbulence. *Phys. Fluids A* **3**: 155–162.

Zeman O. 1981. Progress in the modeling of planetary boundary-layers. *Annu. Rev. Fluid Mech.* **13**: 253–272.

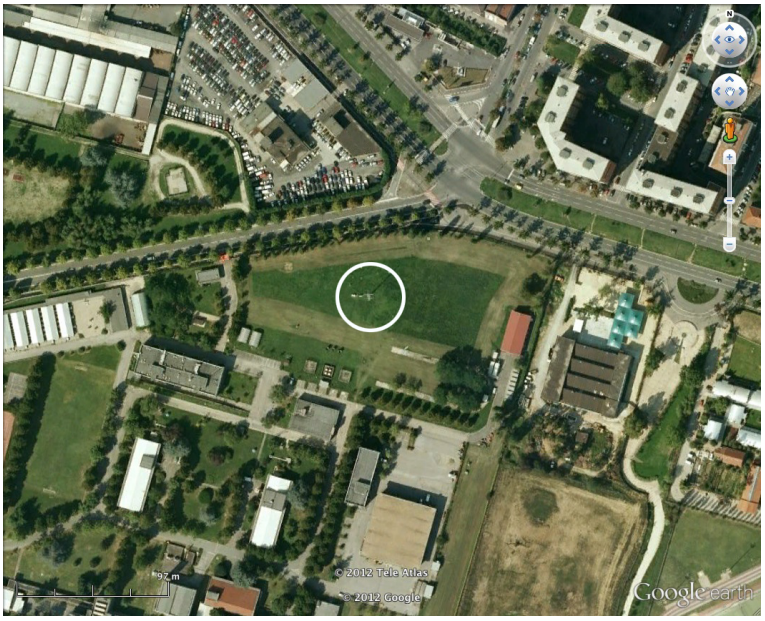

Figure 1. Satellite view of the measurement area. The circle indicates the mast.

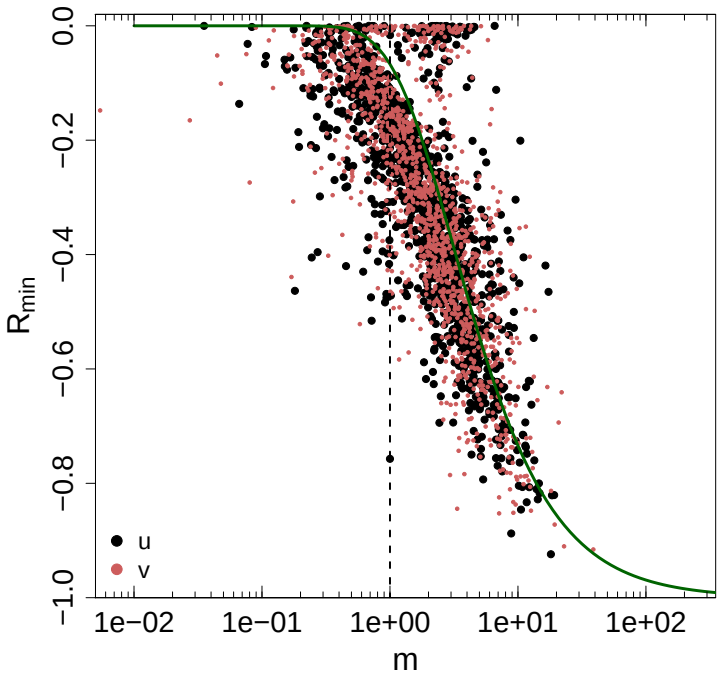

Figure 2. R_{min} as a function of m at 5 m evaluated from stationary data. The Continuous line refers to eq. (7), the dashed line corresponds to $m = 1$, dots refer to u and v components, respectively.

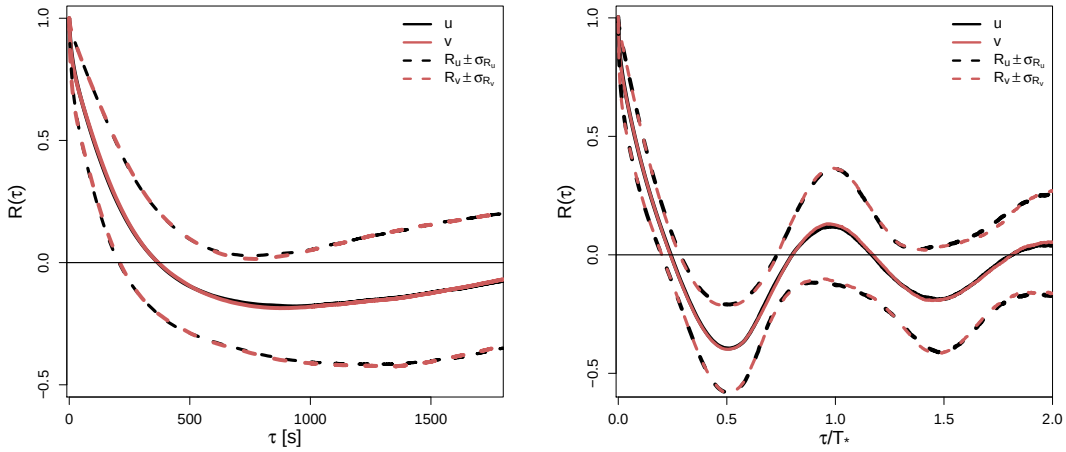

(a) (b)

Figure 3. EAFs averaged over all the data set at 5 m. Cases in which $m > 1$ and $\overline{u} < 1.5\, ms^{-1}$ considered only. Solid lines refer to u and v components, whereas the dashed lines indicate $\pm$ a standard deviation. Left panel shows $R(\tau)$ vs τ, while in the right panel $R(\tau)$ vs τ/T_* are plotted

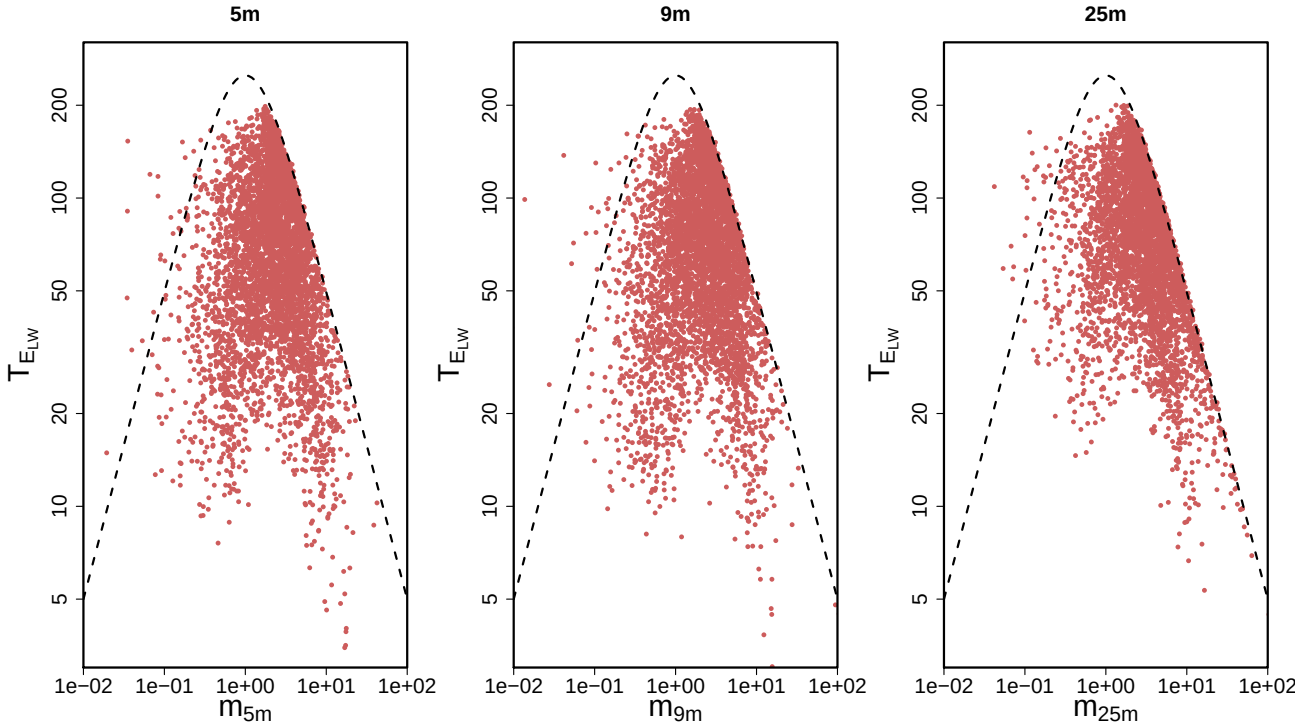

Figure 4. Eulerian time scale, in s, evaluated with Eq. (8) as a function of q and m for the three heights. The dashed line refers to the the function $\frac{m}{q_{min}(1+m^2)}$, where q_{min} represents the minimum value of q_i for $m \geq 1$.

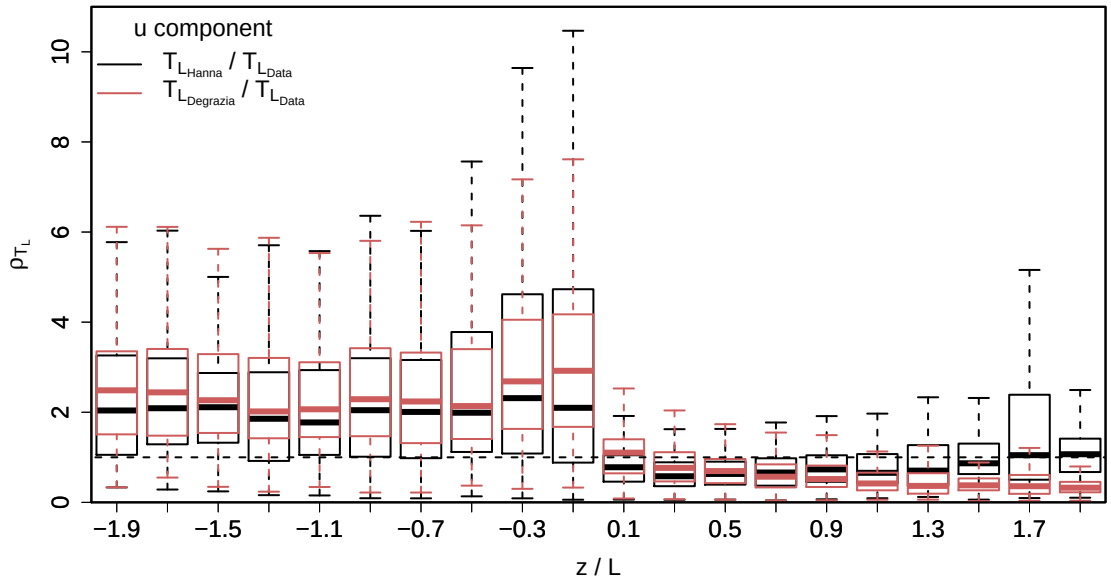

(a) 25m u component

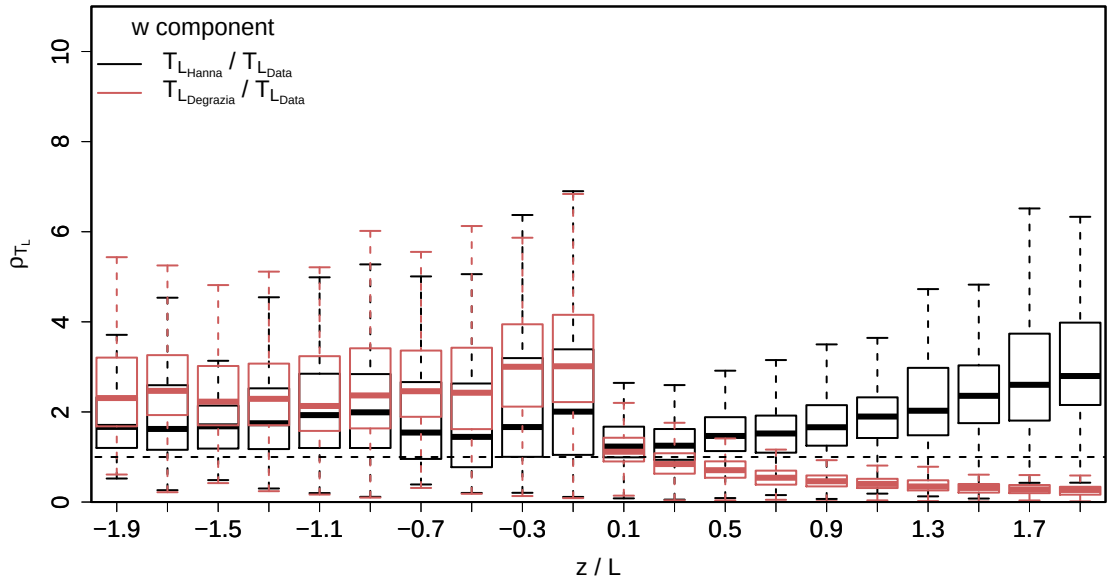

(b) 25m w component

Figure 5. Ratio of parameterized and evaluated Lagrangian time scales, ρ_{T_L}, as a function of stability. For each stability class a boxplot is shown.

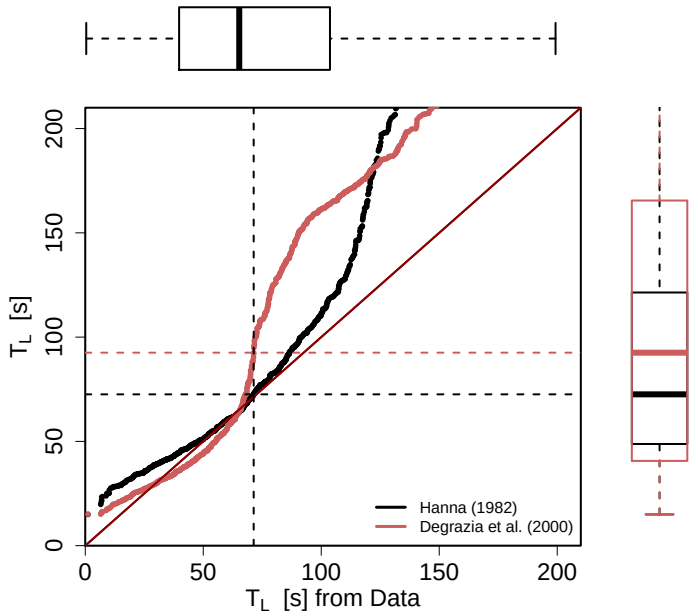

Figure 6. Quantile-quantile plots of the evaluated and parameterized Lagrangian time Scales (Degrazia *et al.* 2000; Hanna 1982), u component at 25 m. Along each axis the correspondent boxplot is depicted to show the quantile distribution among the values.

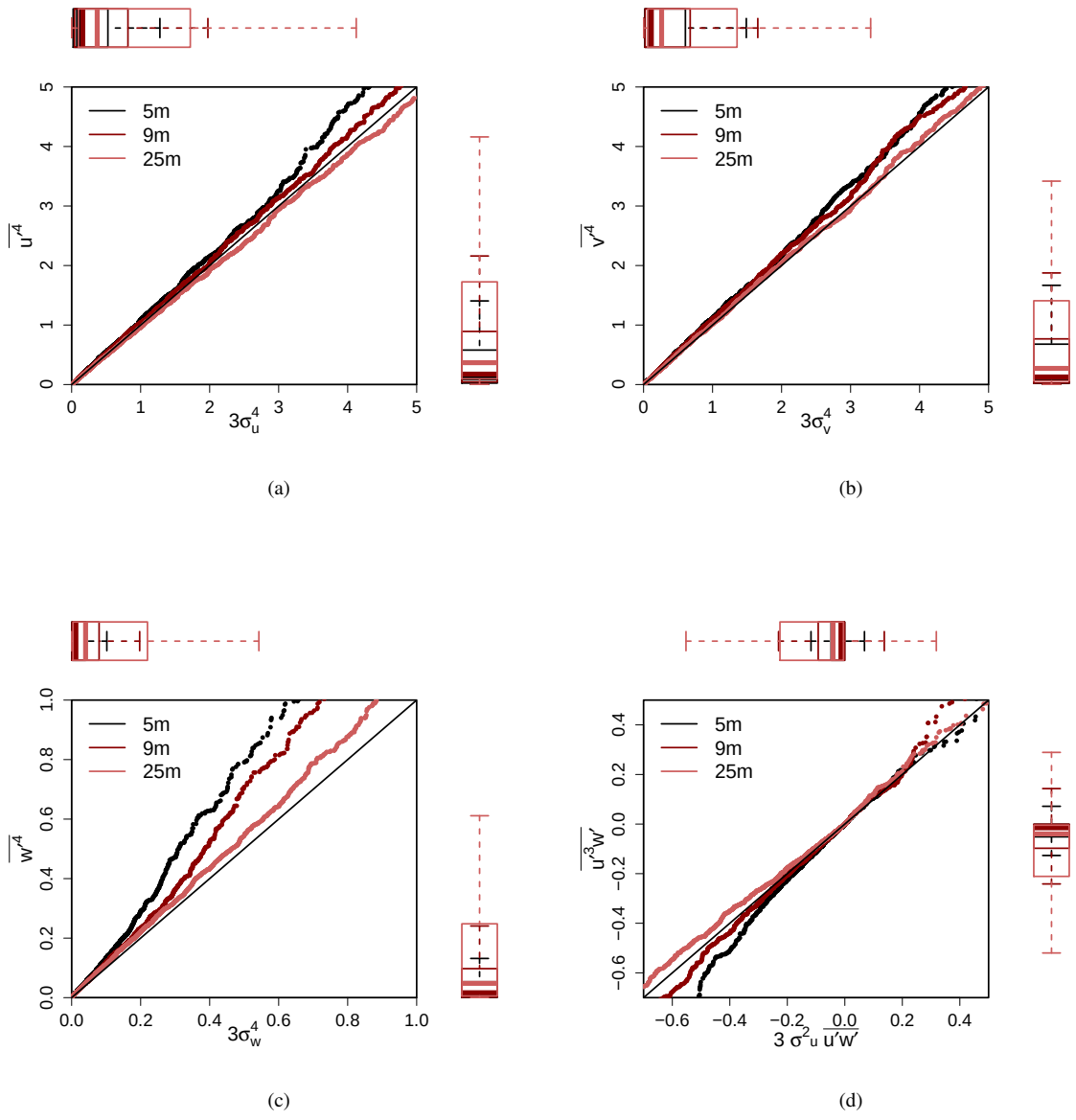

Figure 7. Quantile-quantile plot of the three wind components centered fourth moments versus their quasi-normal approximations for the three heights. (a) $\overline{u'^4}$, (b) $\overline{v'^4}$, (c) $\overline{w'^4}$, (d) $\overline{u'^3w'}$. Along each axis the corresponding boxplot is shown.

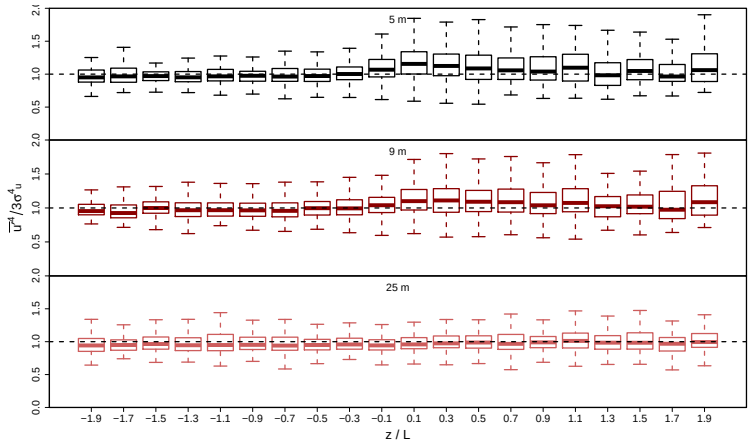

(a) $\frac{\overline{u'^4}}{3\sigma_u^4}$ as a function of stability for the three heights

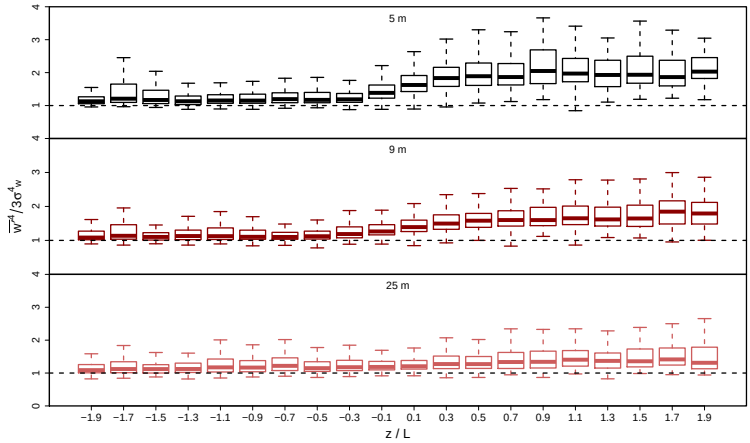

(b) $\frac{\overline{w'^4}}{3\sigma_w^4}$ as a function of stability for the three heights

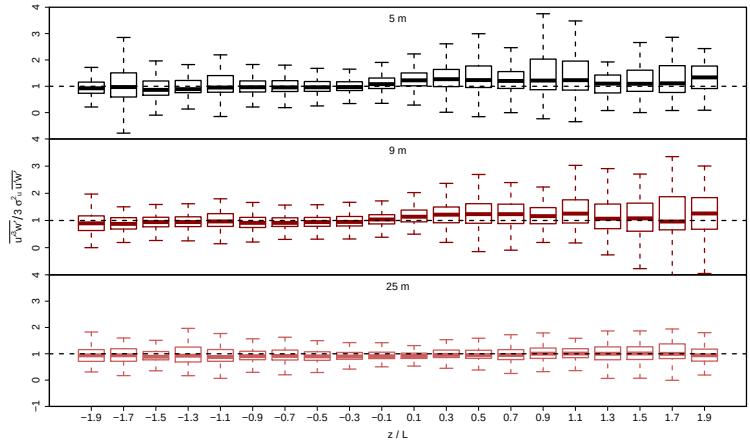

(c) $\frac{\overline{u'^3 w'}}{3\sigma_u^2 \overline{u'w'}}$ as a function of stability for the three heights

Figure 8. Boxplots of the ration between the fourth-moments evaluated from the data and their quasi-normal approximations.

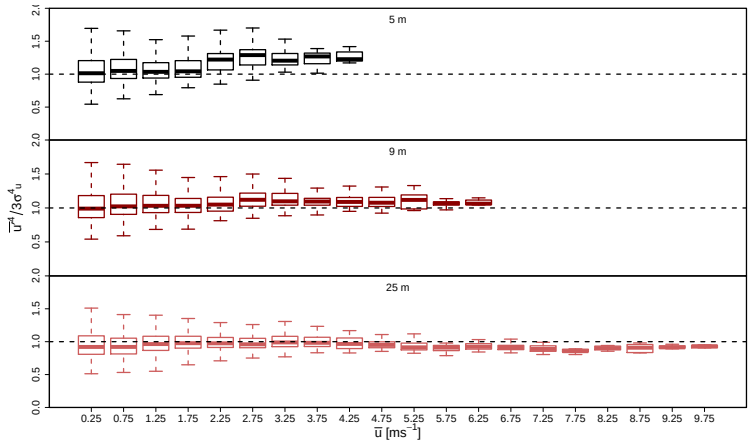

(a) $\frac{\overline{u'^4}}{3\sigma_u^4}$ as a function of the mean velocity $\overline{u}$ for the three heighs

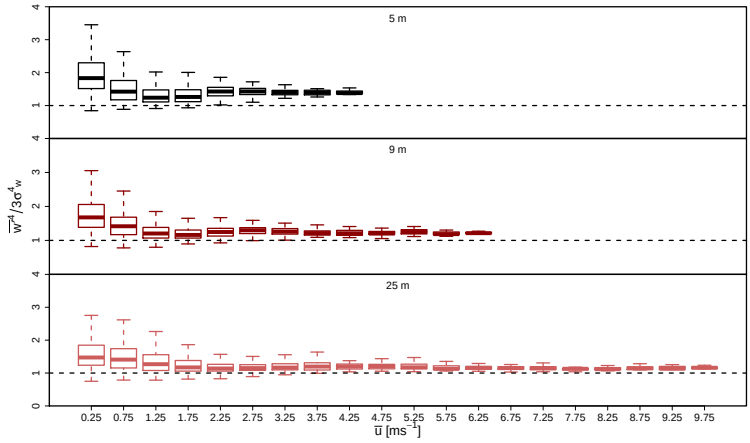

(b) $\frac{\overline{w'^4}}{3\sigma_w^4}$ as a function of the mean velocity $\overline{u}$ for the three heights

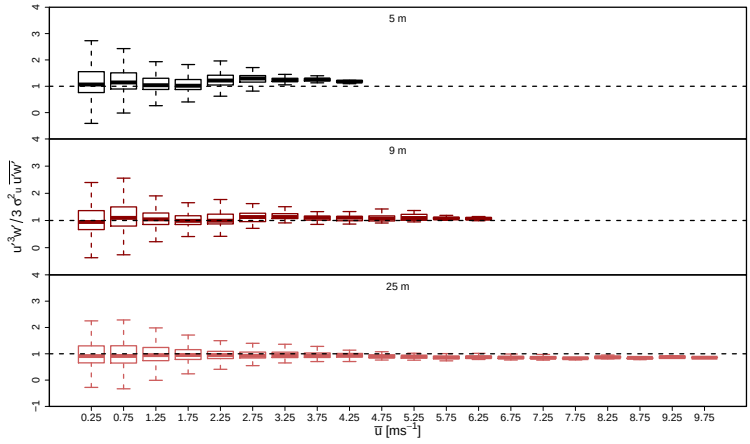

(c) $\frac{\overline{u'^3w'}}{3\sigma_u^2\overline{u'w'}}$ as a function of the mean velocity $\overline{u}$ for the three heights

Figure 9. Boxplots of the ration between the fourth-moments evaluated from the data and their quasi-normal approximations.

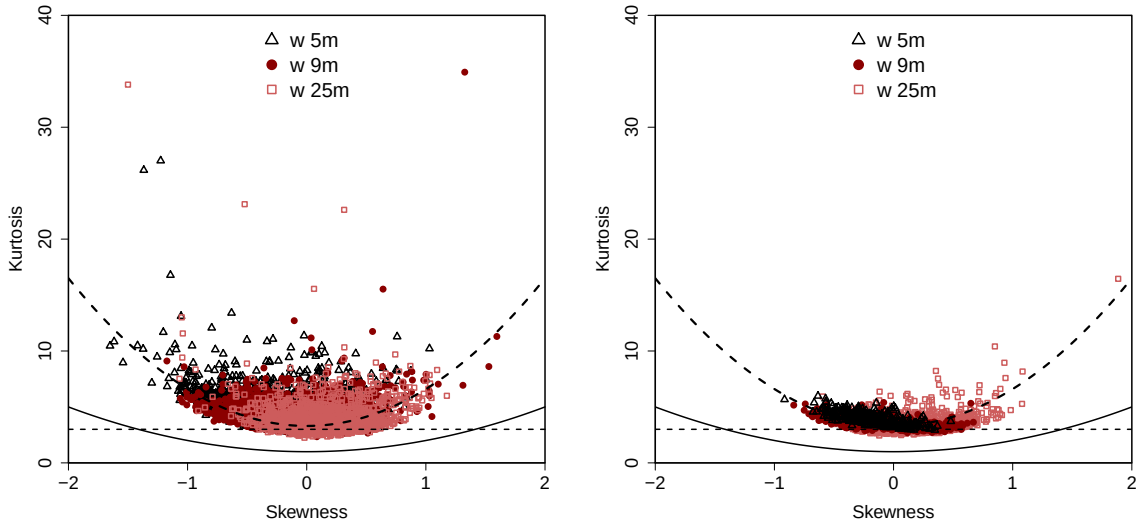

Figure 10. Vertical velocity kurtosis as a function of the skewness for low (a) and strong (b) wind conditions. △ 5m data, • 9m data, □ 25m data. The dashed line represents Eq. (13) with $\alpha = 3.3$, the solid line is the statistical limit, while the horizontal dotted line is the Gaussian value.

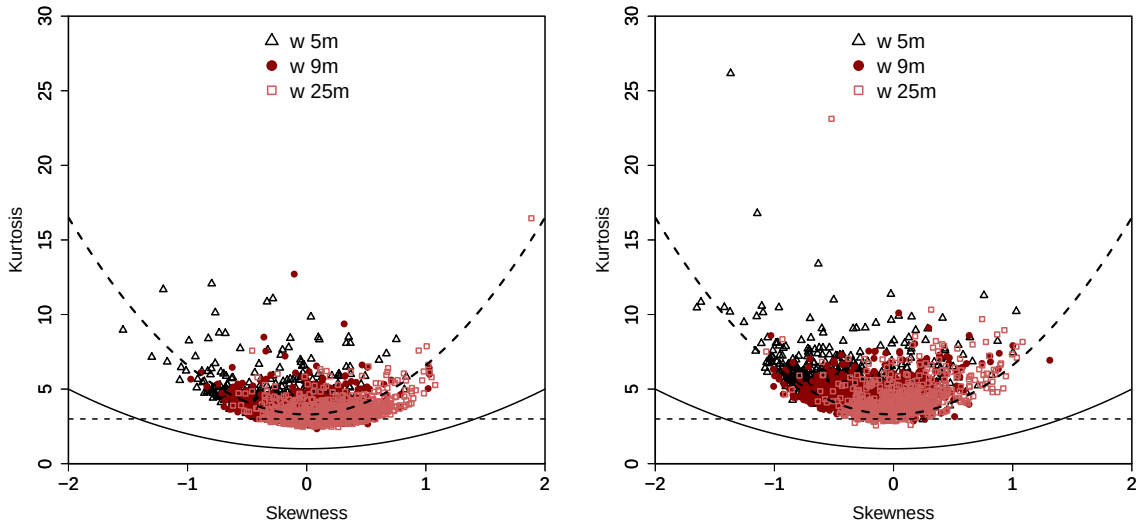

Figure 11. Vertical velocity kurtosis as a function of the skewness for unstable (a) and stable (b) conditions. △ 5m data, • 9m data, □ 25m data.The dashed line represents Eq. (13) with $\alpha = 3.3$, the solid line is the statistical limit, while the horizontal dotted line is the Gaussian value.